Analysis of Differential Conditioning of Erogodic Cellular Automaton Neruon Model

ISHIKAWA, Masato

(出版者 / Publisher)
法政大学大学院理工学研究科
(雑誌名 / Journal or Publication Title)
法政大学大学院紀要. 理工学研究科編
(巻 / Volume)
63
(開始ページ / Start Page)
1
(終了ページ / End Page)
5
(発行年 / Year)
2022-03-24
(URL)
https://doi.org/10.15002/00025314

Analysis of Differential Conditioning of Erogodic Cellular Automaton Neruon Model

<*Name*: Masato ISHIKAWA>

<*Major*: Electrical and Electronic Engineering Major>,

Graduate School of Science and Engineering, Hosei Universit

<*Supervisor*: Hiroyuki Torikai>

***Abstract*-A novel membrane potential model whose nonlinear dynamics is described by an ergodic discrete difference equation is presented. Detailed analyses reveal that the ergodicity of the model plays an important role to realize proper generations of action potentials. Then, using the ergodic membrane potential model, a novel multi-compartment neuron model (soma-dendrite-synapse model) is presented. It is shown that the model can exhibit various dendritic phenomena depending on parameter values. Based on detailed analyses of the dendritic phenomena, a design procedure of the multi-compartment neuron model to realize conditioning functions is proposed. Furthermore, the neuron model is implemented by a field programmable gate array and experiments validate its conditioning functions. It is then shown that the proposed neuron model consumes much fewer hardware resources and much lower power than a typical conventional multi-compartment neuron model.**

Keyward: Multi-Compartment Neuron Model, Ergodic Sequential logic, STDP, Differential Conditioning, FPGA

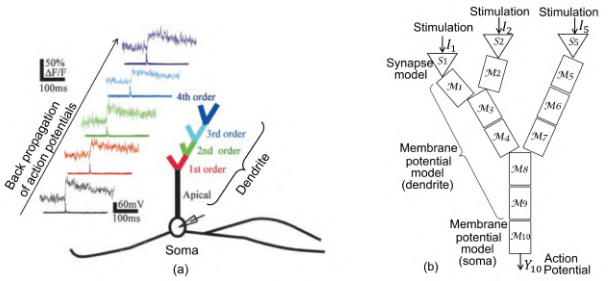

Fig. 1. (a) Backward propagation of action potentials on dendrite of a biological in vivo *neuron [6]. (b) Multi-compartment modeling method of neuron.*

I. INTRODUCTION

A biological neuron typically consists of a soma, dendrites, synapses, and axons as illustrated in Fig. 1(a). The biological neuron exhibits a wide variety of dendritic phenomena such as forward and backward propagations of action potentials and their combinations [1]-[5], e.g., Fig. 1(a) shows a typical example of backward propagation of action potentials on the dendrite of a biological *in vivo* neuron [6]. It has been pointed out that the physical structure of the dendrite and corresponding dendritic propagation phenomena of action potentials play important roles in information processing and learning of biological neuron networks [4][5][7]-[10]. A major modeling method is the multi-compartment modeling method [11]-[14], by which the neuron is modeled as a coupled system of small compartments as illustrated in Fig. 1(b). There are some methods to mode electronic circuit multi-compartment soma-dendrite model. One of the method is a ergodic *discrete difference equation* (DDE) [15]. The ergodic DDE has a continuous state transition time and discrete state space. A model designed by this model can be implemented by a sequential logic circuit driven by ergodic binary signals. It has been shown that ergodic DDE neuromorphic circuits have consumed much fewer hardware resources and much lower power compared to digital-processor-based neuromorphic circuits [15]. In this paper, a multi-compartment

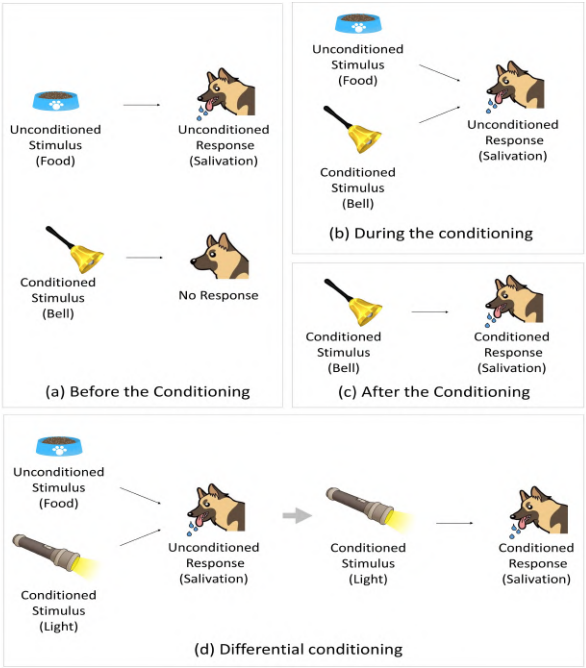

Fig. 2. Illustrations of differential classical conditioning and extinction. (a) Before conditioning. (b) During the conditioning. (c) After the conditioning. This phenomenon is called classical conditioning. (d) If the animal can be conditioned by multiple conditioned stimuli (e.g., bell and light) selectively, the animal is said to realize differential classical conditioning.

soma-dendrite-synapse model based on the nonlinear dynamics of an ergodic DDE is presented. Using the model, a typical classical conditioning function (i.e., differential classical conditioning [16][17], see also Fig. 2) is realized. In addition, the presented model is implemented by a field programmable gate array. It is then shown that the presented model consumes much fewer hardware resources and much lower power than a typical conventional multi-compartment neuron model [18].

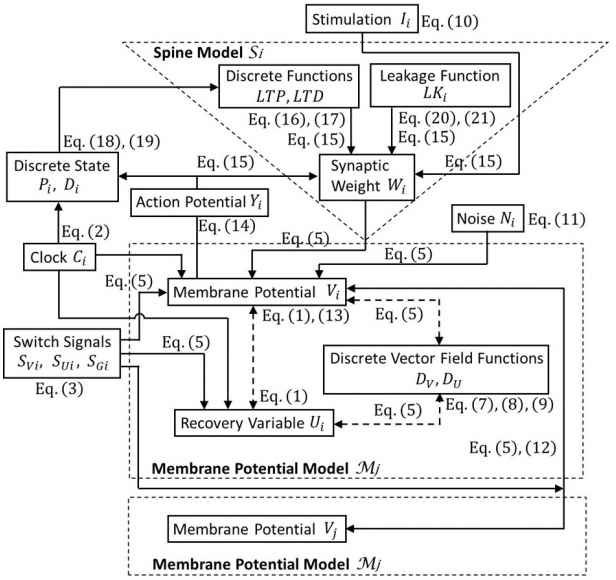

Fig. 3. Schematic diagrams of novel ergodic DDE membrane potential model $\mathcal{M}_i$, synapse model $\mathcal{S}_i$, and conductance-type coupling G_{ij}. "LUT" represents "lookup table."

II. Novel Ergodic DDE Membrane Potential Model

In this section, a novel discrete difference equation (DDE) membrane potential model is presented. Fig. 3 shows a schematic diagram of the model denoted by $\mathcal{M}_i$, where i is an integer index. The i-th membrane potential model $\mathcal{M}_i$ has two registers storing the following discrete states.

$$\begin{aligned} &\text{Discrete membrane potential} \\ &\qquad V_i \in \{0, 1, \cdots, M-1\} = \boldsymbol{M}, \\ &\text{Discrete recovery variable} \\ &\qquad U_i \in \{0, 1, \cdots, N-1\} = \boldsymbol{N}. \end{aligned} \tag{1}$$

The membrane potential model $\mathcal{M}_i$ has a periodic clock

$$C_i(t) = \sum_{n=0}^{\infty} p(t - nT_{Ci}), \tag{2}$$

where $p(t)$ represents an instantaneous pulse defined by $p(t) = 1$ if $t = 0$ and $p(t) = 0$ if $t \neq 0$, and $T_{Ci} > 0$ is a period of $C_i(t)$. The membrane potential model $\mathcal{M}_i$ also has the following three binary switch signals.

$$\begin{aligned} S_{Vi}(t) &= \sum_{n=0}^{\infty} q(t - nT_{Vi} - \Phi_{Vi}, Q_{Vi}), \\ S_{Ui}(t) &= \sum_{n=0}^{\infty} q(t - nT_{Ui} - \Phi_{Ui}, Q_{Ui}), \\ S_{Gi}(t) &= \sum_{n=0}^{\infty} q(t - nT_{Gi} - \Phi_{Gi}, Q_{Gi}), \end{aligned} \tag{3}$$

where $q(t, Q)$ represents a pulse defined by

$$q(t) = \begin{cases} 1 & \text{if } t \in (0, Q], \\ 0 & \text{if } t \notin (0, Q], \end{cases} \tag{4}$$

$T_{Vi} > 0, T_{Ui} > 0$, and $T_{Gi} > 0$ are periods; $Q_{Vi} \in [0, T_{Vi}]$, $Q_{Ui} \in [0, T_{Ui}]$, and $Q_{Gi} \in [0, T_{Gi}]$ are pulse durations; and $\Phi_{Vi} \in [0, T_{Vi})$, $\Phi_{Ui} \in [0, T_{Ui})$, and $\Phi_{Gi} \in [0, T_{Gi})$ are initial phases. The internal clock $C_i(t)$ triggers the following transitions of the discrete states V_i and U_i (see also Fig. 3):

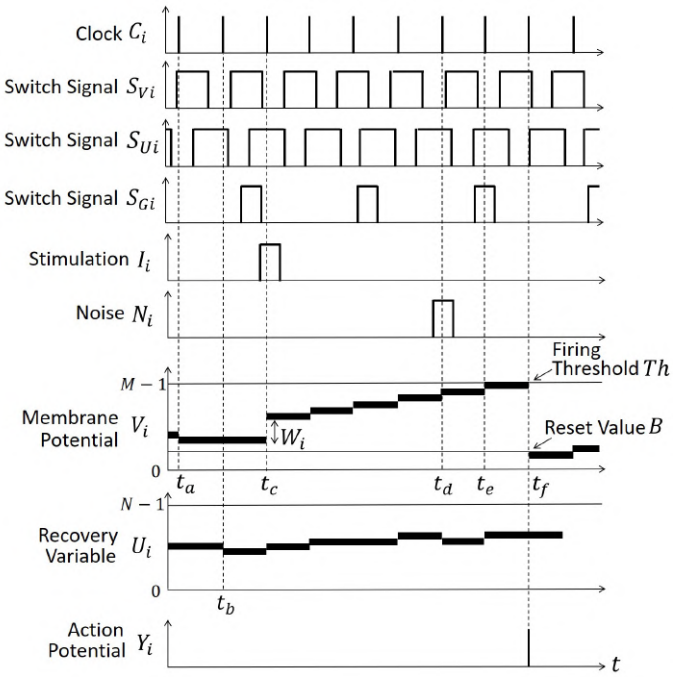

Fig. 4. State transitions of the ergodic DDE membrane potential model $\mathcal{M}_i$.

$$\begin{aligned} &\text{If } C_i(t) = 1, \text{ then} \\ &\begin{cases} V_i(t^+) = V_i(t) + S_{Vi}(t) D_V(V_i(t), U_i(t)) + N_i(t) \\ \qquad\qquad + R_i(V_i(t)) W_i I_i(t) \\ \qquad\qquad + S_{Gi}(t) G_{ij}(V_j(t) - V_i(t)), \\ U_i(t^+) = U_i(t) + S_{Ui}(t) D_U(V_i(t), U_i(t)), \end{cases} \end{aligned} \tag{5}$$

where $t^+ = \lim_{\epsilon \to +0} t + \epsilon$. Additionally, V_i (U_i) is assumed to be saturated at 0 and $M-1$ (0 and $N-1$) and is assumed to exist in its range $\boldsymbol{M}$ (range $\boldsymbol{N}$). The function $R_i(V_i) \in \{0, 1\}$ represents refractoriness of a neuron and is defined by

$$R_i(V_i) = \begin{cases} 0 & \text{if } V > V_r, \\ 1 & \text{otherwise.} \end{cases} \tag{6}$$

The state transitions in Eq. (5) consist of the following four types of transitions.

(1) Transition by vector field: In Eq. (5), $D_V(V_i, U_i) : \boldsymbol{M} \times \boldsymbol{N} \to \{-1, 0, 1\}$ and $D_U(V_i, U_i) : \boldsymbol{M} \times \boldsymbol{N} \to \{-1, 0, 1\}$ are discrete functions, which determine the nonlinear vector field of the membrane potential model $\mathcal{M}_i$. Hence D_V and D_U are referred to as discrete vector field functions. The discrete vector field functions D_V and D_U are implemented by logic gates or lookup tables. In this paper, to realize various dendritic phenomena, the discrete vector field functions D_V and D_U are designed as follows:

$$D_V(V_i, U_i) = \begin{cases} 1 & \text{if } (V_i, U_i) \in \mathbf{S}_i^{++} \cup \mathbf{S}_i^{+-}, \\ -1 & \text{if } (V_i, U_i) \in \mathbf{S}_i^{-+} \cup \mathbf{S}_i^{--}, \\ 0 & \text{if } (V_i, U_i) \in \mathbf{S}_i^{0}, \end{cases} \tag{7}$$

$$D_U(V_i, U_i) = \begin{cases} 1 & \text{if } (V_i, U_i) \in \mathbf{S}_i^{++} \cup \mathbf{S}_i^{-+}, \\ -1 & \text{if } (V_i, U_i) \in \mathbf{S}_i^{+-} \cup \mathbf{S}_i^{--}, \\ 0 & \text{if } (V_i, U_i) \in \mathbf{S}_i^{0}, \end{cases} \tag{8}$$

$$
\begin{aligned}
&\mathbf{S}_i^{++} \equiv \{(V_i, U_i) | U_i < f_V(V_i), U_i \le f_U(V_i)\},\\
&\mathbf{S}_i^{-+} \equiv \{(V_i, U_i) | U_i \ge f_V(V_i), U_i < f_U(V_i)\},\\
&\mathbf{S}_i^{+-} \equiv \{(V_i, U_i) | U_i \le f_V(V_i), U_i > f_U(V_i)\},\\
&\mathbf{S}_i^{--} \equiv \{(V_i, U_i) | U_i > f_V(V_i), U_i \ge f_U(V_i)\},\\
&\mathbf{S}_i^{0} \equiv \{(V_i, U_i) | (V_i, U_i) \notin \mathbf{S}_i^{++} \cup \mathbf{S}_i^{+-} \cup \mathbf{S}_i^{-+} \cup \mathbf{S}_i^{--}\},
\end{aligned} \tag{9}
$$

$f_V(V_i) = \lfloor k_1(V_i)^2 + k_2 V_i + k_3 \rfloor$, $f_U(V_i) = \lfloor k_4 V_i + k_5 \rfloor$, $k_1 = f_1 M/N^2$, $k_2 = -2k_1\lfloor f_2 N \rfloor$, $k_3 = k_1(\lfloor f_2 N \rfloor)^2 + \lfloor f_3 M \rfloor$, $k_4 = f_4 M/N$, $k_5 = \lfloor f_5 M \rfloor$, and $\lfloor \cdot \rfloor$ is the floor function. In Fig. 3, the discrete states V_i and U_i are transited by the vector field functions D_V and D_U at the moments $t = t_a$ and t_b when the clock $C_i = 1$ arrives, respectively.

(2) Transition by stimulation: As shown in Fig. 3, the membrane potential model $\mathcal{M}_i$ receives a discrete synaptic weight $W_i \in \{0, 1, \cdots, W_{max}\}$ if a synapse model $\mathcal{S}_i$ is connected. The synapse model $\mathcal{S}_i$ receives a pulse stimulation

$$
I_i(t) = \sum_{n=1}^{\infty} q(t - t_{Ii}(n), Q_{Ii}), \tag{10}
$$

where $t_{Ii}(n)$ represents the n-th pulse timing of $I_i(t)$. In Fig. 4, the discrete state V_i is transited by the weighted stimulation $W_i I_i(t)$ at the moment $t = t_c$ when the clock $C_i = 1$ arrives.

(3) Transition by noise: As shown in Fig. 3, the membrane potential model $\mathcal{M}_i$ receives a pulse noise

$$
N_i(t) = \sum_{n=1}^{\infty} q(t - t_{Ni}(n), Q_{Ni}), \tag{11}
$$

where $t_{Ni}(n)$ represents the n-th pulse timing of $N_i(t)$. In Fig. 4, the discrete state V_i is transited by the noise $N_i(t)$ at the moment $t = t_d$ when the clock $C_i = 1$ arrives.

(4) Transition by coupling: As shown in Fig. 3, assume the membrane models $\mathcal{M}_i$ and $\mathcal{M}_j$ are coupled. In Eq. (5), $G_{ij} : \{-(M-1), -(M-2), \cdots, M-1\} \to \{-(M-1), -(M-2), \cdots, M-1\}$ is a discrete function, which determines the characteristics of the coupling. Hence G_{ij} is referred to as a coupling function. In this paper, to realize various dendritic phenomena, the coupling function G_{ij} is designed as follows:

$$
G_{ij}(V) = \begin{cases} \lfloor g_{ij} V \rfloor & \text{if } -T_{ij} \le V \le 0, \\ 0 & \text{otherwise,} \end{cases} \tag{12}
$$

where $T_{ij} \in \boldsymbol{M}$ and $g_{ij} \in \boldsymbol{R}$ are parameters. In Fig. 4, the discrete state V_i is transited by the coupling function G_{ij} at the moment $t = t_e$ when the clock $C_i = 1$ arrives.

In addition to the transitions in Eq. (5), the membrane potential model $\mathcal{M}_i$ exhibits the following firing reset.

$$
\begin{aligned}
&\text{If } C_i(t) = 1 \text{ and } V_i(t) = Th(U_i),\\
&\qquad \text{then } V_i(t^+) = B(U_i),
\end{aligned} \tag{13}
$$

where $Th : \boldsymbol{N} \to \boldsymbol{M}$ is a firing threshold and $B : \boldsymbol{N} \to \boldsymbol{M}$ is a reset value. In Fig. 4, the model $\mathcal{M}_i$ exhibits the firing reset at the moment $t = t_f$. At the firing moment, the model $\mathcal{M}_i$ generates the following action potential (see also Fig. 3):

$$
Y_i(t) = \begin{cases} 1 & \text{if } V_i(t) = Th(U_i) \text{ and } C_i(t) = 1, \\ 0 & \text{otherwise.} \end{cases} \tag{14}
$$

A. *Spike timing dependent synaptic plasticity of synapse model*

To realize the conditioning functions of the neuron model, the synapse model $\mathcal{S}_i$ is extended to realize plasticity of the synaptic weight W_i as follows:

$$
\begin{aligned}
&\text{If } C_i(t) = 1, \text{ then}\\
&W_i(t^+) = W_i(t) + Y_i(t) I_{k(i)}(t) LTP(P_i(t))\\
&\qquad - I_i(t) LTD(D_i(t)) - LK_i(K_i(t)),
\end{aligned} \tag{15}
$$

where W_i is assumed to be saturated at 0 and W_{max} and to exist in its range. Also, $P_i \in \{0, 1, \cdots, P_{max}\}$ and $D_i \in \{0, 1, \cdots, D_{max}\}$ are discrete states, and $LTP : \{0, \cdots, P_{max}\} \to \{0, 1\}$ and $LTD : \{0, \cdots, D_{max}\} \to \{0, 1\}$ are discrete functions defined by

$$
LTP(P) = \begin{cases} 0 & \text{if } P = 0, \\ 1 & \text{if } P > 0, \end{cases} \tag{16}
$$

$$
LTD(D) = \begin{cases} 0 & \text{if } D = 0, \\ 1 & \text{if } D > 0. \end{cases} \tag{17}
$$

The dynamics of the discrete states P_i and D_i are:

$$
\begin{aligned}
&P_i(t^+) = P_{max} && \text{if } C_i(t) = 1 \text{ and } I_i(t) = 1,\\
&P_i(t^+) = P_i(t) - 1 && \text{if } C_i(t) = 1,
\end{aligned} \tag{18}
$$

$$
\begin{aligned}
&D_i(t^+) = D_{max} && \text{if } C_i(t) = 1 \text{ and } Y_i(t) = 1,\\
&D_i(t^+) = D_i(t) - 1 && \text{if } C_i(t) = 1,
\end{aligned} \tag{19}
$$

where P_i (D_i) is assumed to be saturated at 0 and P_{max} (0 and D_{max}) and to exist in its range. The functions LTP and LTD work to increase the synaptic weight W_i (i.e., long-term potentiation) and to decrease the synaptic weight W_i (i.e., long-term depression), respectively. Using the extended synapse model $\mathcal{S}_i$, the synaptic weight W_i is increased if an action potential $Y_i = 1$ (i.e., post-synaptic spike) comes to the synapse model $\mathcal{S}_i$ after a stimulation $I_i = 1$ (i.e., pre-synaptic spike) comes, and is decreased in the opposite case. In addition, $K_i \in \{0, 1, \cdots, K_{max}\}$ is a discrete state and $LK : \{0, \cdots, K_{max}\} \to \{0, 1\}$ is a discrete function defined by

$$
LK_i(K) = \begin{cases} \Lambda_i & \text{if } K = K_{max}, \\ 0 & \text{otherwise.} \end{cases} \tag{20}
$$

The dynamics of the discrete state K_i is:

$$
\begin{aligned}
&K_i(t^+) = K_i(t) + 1 && \text{if } C_i(t) = 1 \text{ and } K_i(t) < K_{max},\\
&K_i(t^+) = 0 && \text{if } C_i(t) = 1 \text{ and } K_i(t) = K_{max}\\
&&& \text{or } C_i(t) = 1 \text{ and } Y_i(t) = 1.
\end{aligned} \tag{21}
$$

The function LK work as leakage of the synaptic weight W_i.

III. RESULTS

A. *Differential classical conditioning*

Recall that, in the differential classical conditioning explained in Fig. 2, an unconditioned stimulus (e.g., food) and multiple conditioned stimuli (e.g., bell and light) are used, where the unconditioned stimulus leads to an innate

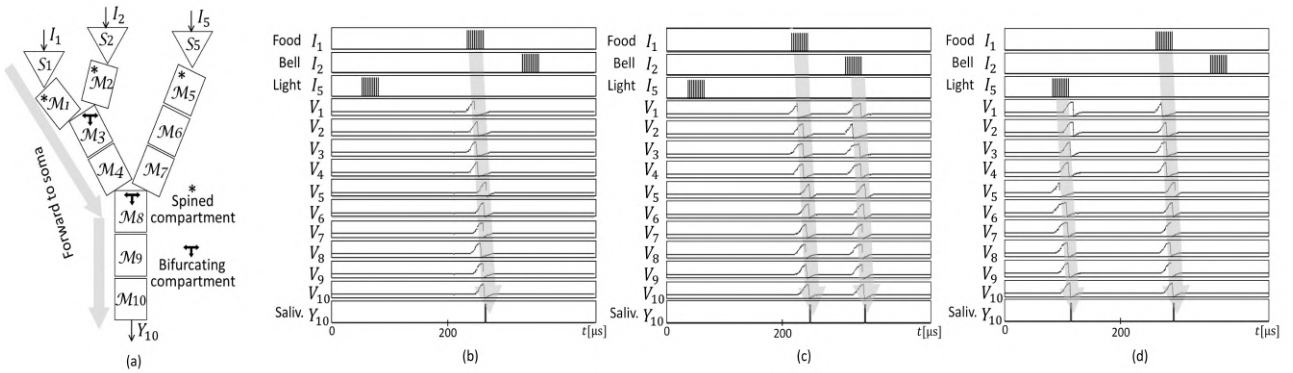

Fig. 5. Differential conditioning of the multi-compartment neuron model. (a)Proposed multi-compartment neuron model. (b),(c), and (d) are simulation results showing typical time waveforms of the model before and after conditioning. The parameter values of the membrane model are $(M, N, f_1, f_2, f_3, f_4, f_5) = (64, 64, 3.5, 0.45, -0.05, 1.5, -0.43)$*,* $Th = 63$*,* $B = 0$*,* $T_{Ci} = T_{Vi} = Q_{Vi} = Q_{Ui} = Q_{Gi} = 121$*,* $T_{Ui} = 12\sqrt{817}$*, and* $T_{Gi} = 4\sqrt{770}$*,* $V_r = 63$*. The coupling functions* G_{ij} *are parameterized as* $g_{31} = g_{32} = g_{43} = g_{65} = g_{76} = g_{84} = g_{87} = g_{98} = g_{109} = 0.5$ *and* $g_{13} = g_{23} = g_{34} = g_{56} = g_{67} = g_{48} = g_{78} = g_{89} = g_{910} = 0.5$*. Pulse density of the noise* N_i *is* $20\sqrt{259}$*. The parameter values of the synapse model are* $(P_{max}, D_{max}, W_{max}, \alpha, \beta) = (500, 250, 10, 0.5, 0.5)$*,* $V_r = 63$*, and* $W_1 = 10$*. (a) Before conditioning.* $W_2 = W_5 = 0$*. (b) After conditioned by the bell stimulation* I_2*.* $W_2 = 10$ *and* $W_5 = 0$*. (c) After conditioned by the light stimulation* I_5*.* $W_2 = 0$ *and* $W_5 = 10$*.*

Table 1. Comparisons.

Model	Function		Hardware				
	Differential conditioning	Extinction	Resolusions of discrete state	#LUTs	#FFs	#Slices	On-chip power [W]
Presented neuron model operated as ergodic DDE	Possible	Possible	N=64 M=64	1492	371	459	0.141
Presented neuron model operated as regular DDE	Not suited as explained in Remarks 1 and 2		N=64 M=64	1561	533	521	0.138
Neuron model described by ODE	Possible	Possible	19bit	16851	779	5551	0.586

#LUTs, #FFs and #Slices represent the numbers of FPGA of lookup tables, of flip flops and of slices respectively.

response (e.g., salivation) regardless of the conditioning. In this paper, a design method of the multi-compartment neuron model in Fig. 5(a) to realize the differential classical conditioning with two conditioned stimuli is proposed. Fig. 5(b) shows typical time waveforms of the multi-compartment neuron model designed by the above method before conditioning. In this figure, the neuron model salivates (i.e., the soma generates $Y_{10} = 1$) in response to the food stimulation $I_1 = 1$ but does not to the bell stimulation $I_2 = 1$ or the light stimulation $I_5 = 1$. The neuron model is then conditioned by giving the food stimulation $I_1 = 1$ and the bell stimulation $I_2 = 1$ repeatedly and randomly, where the food stimulation is presented near the bell stimulation. Fig. 5(c) shows typical time waveforms of the neuron model after the conditioning. In this figure, the neuron model salivates $Y_{10} = 1$ in response to the food stimulation $I_1 = 1$ and the bell stimulation $I_2 = 1$ but does not to the light stimulation $I_5 = 1$. On the other hand, in the case of Fig. 5(d), the neuron model is conditioned by giving the food stimulation $I_1 = 1$ and the light stimulation $I_5 = 1$. After this conditioning, as shown in Fig. 5(d), the neuron model salivates $Y_{10} = 1$ in response to the food stimulation $I_1 = 1$ and the light stimulation $I_5 = 1$ but does not to the bell stimulation $I_2 = 1$. These results reveal that the neuron model can pair the unconditioned food stimulation I_1 with the conditioned bell stimulation I_2 or with the conditioned

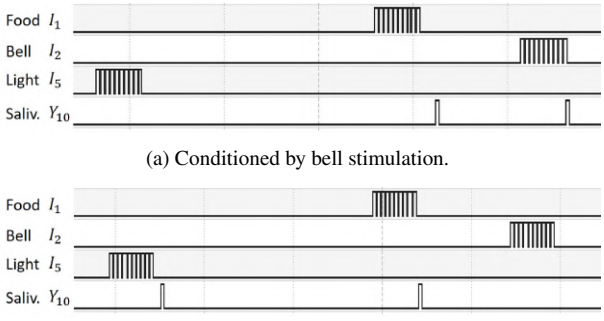

(a) Conditioned by bell stimulation.

(b) Conditioned by light stimulation.

Fig. 6. Oscilloscope snapshots of the presented multi-compartment neuron model implemented by Xilinx's FPGA device XC7Z020-1CLG484. The scale of the horizontal time axis is 200 ms/div.. (a) Conditioned by bell stimulation corresponding to Fig. 5(b). (b) Conditioned by light stimulation corresponding to Fig. 5(c).

light stimulation I_5 selectively, and thus it can be said that the neuron model can realize the differential conditioning.

B. *FPGA Implementation and Comparison*

The set of the dynamic equations (5)-(15) describing the multi-compartment neuron model in Fig. 5(a) was hand-written as a register transfer level Verilog-HDL code. The code was compiled by Xilinx's design software environment Vivado Design Suite 2019.2.1 and the resulting bit-

stream file was downloaded to Xilinx's field programmable gate array (FPGA) XC7Z020-1CLG484. Fig. 6 shows oscilloscope snapshots of the multi-compartment neuron model after the differential conditioning. In Fig. 6(a), the model was conditioned by the bell stimulation. It can be seen in the figure that the model salivates (i.e., Y_{10} = High) in response to the food stimulation I_1 = High and the bell stimulation I_2 = High but does not to the light stimulation I_5 = High. In Fig. 6(b), the model was conditioned by the light stimulation. It can be seen in the figure that the model salivates in response to the food stimulation I_1 = High and the light stimulation I_5 = High but does not to the bell stimulation I_2 = High. Hence the model realizes the differential conditioning properly.

For comparison, a multi-compartment neuron model having the in structure in Fig. 5(a) and composed of the following ordinary differential equation (ODE) membrane model [14] was designed.

$$\begin{aligned} &Cdv/dt = k(v - v_r)(v - v_t) - u + I \\ &du/dt = a\{b(v - v_r) - u\} \\ &\begin{cases} v = c \\ u = u + d \end{cases} \quad \text{if } v \geq v_{peak}. \end{aligned} \tag{22}$$

where $v_i \in \boldsymbol{R}$ is a membrane potential and $u_i \in \boldsymbol{R}$ is a recovery variable, $(k, v_r, v_t, I, C, a, b, c, d, v_{peak}) = (0.7, -60, -40, 0, 100, 0.03, 5, -60, 100, 35)$. The dynamics of the ODE multi-compartment neuron model was transformed into a numerical integration formula, which was implemented by the same design software and in the same FPGA device used to implement the presented model. Table 1 shows comparison results. Note that the bit lengths of the presented ergodic DDE neuron model and the ODE neuron model were shortened as short as possible under the condition that the model realized the differential conditioning properly. It can be confirmed that the presented ergodic DDE neuron model consumes much less hardware resources and much less power compared to the ODE neuron model.

IV. CONCLUSION

It was shown that the presented ergodic DDE membrane potential model could realize the differential conditioning. The designed multi-compartment model was implemeneted by the FPGA and it was shown that the proposed model consumed much fewer hardware resources and much lower power compared to the typical conventional multi-compartment model (see Table 1).

ACKNOWLEDGEMENT

This work was carried out under the direction of my supervisor, Prof. Hiroyuki Torikai at Hosei University. I would like to express my gratitude to him for his persistent support of my work over many years.

REFERENCES

[1] W. R. Chen, et al., Forward and Backward Propagation of Dendritic Impulses and Their Synaptic Control in Mitral cells, Science, vol. 278, no. 5337, pp. 463–467, 1997.
[2] N. Ofer, et al.,, Axonal Tree Morphology and Signal Propagation Dynamics Improve Interneuron Classification, Neuroinform, 2020.
[3] I. Segev, et al., Untangling dendrites with quantitative models, Science, vol. 290, no. 5492, pp. 744-750, 2000.
[4] A. Gidon, et al., Dendritic action potentials and computation in human layer 2/3 cortical neurons, Science, vol. 367, no. 6473, pp. 83-87, 2020.
[5] A. Yuniati and A. D. Ardiyanti, Computational study of action potential initiation and action potential backpropagation in mitral cell of the olfactory bulb, Proc. Int. Conf. on Applied Sciences, Information and Technology, pp. 1-7, 2019.
[6] F. Debarbieux, E. Audinat, and S. Charpak, Action Potential Propagation in Dendrites of Rat Mitral Cells In Vivo, The Journal of Neuroscience, vol. 23, no. 13, pp. 553-3360, July 2, 2003.
[7] J. M. Goaillard, et al., Diversity of Axonal and Dendritic Contributions to Neuronal Output, Front. Cell Neurosci., vol. 13, art. 570, 2020.
[8] P. J. Sjostrom, et al., Dendritic Excitability and Synaptic Plasticity, Physiol. Rev., vol. 88, no. 2, pp. 769–840, 2008.
[9] S Tronel, et al, Spatial learning sculpts the dendritic arbor of adult-born hippocampal neurons, PNAS, vol. 107, no. 17, pp. 7963-7968, April 27, 2010.
[10] M Tripodi, et al, Structural Homeostasis: Compensatory Adjustments of Dendritic Arbor Geometry in Response to Variations of Synaptic Input, PLoS Biol, vol. 6, no. 10, e260, 2008.
[11] I. Segev, et al., The Theoretical Foundation of Dendritic Function, The MIT Press, 2002.
[12] W. Rall, Electrophysiology of a Dendritic Neuron Model, Biophysical Journal, vol. 2, no. 2, pp. 145–167, 1962.
[13] E. Hay, et al., Models of neocortical layer 5b pyramidal cells capturing a wide range of dendritic and perisomatic active properties, PLoS Computational Biology, vol. 7, no. 7, e1002107, 2011.
[14] E. M. Izhikevich, Dynamical Systems in Neuroscience, The MIT Press, 2010.
[15] S. Komaki, K. Takeda and H. Torikai, A Novel Ergodic Discrete Difference Equation Model of Central Pattern Generator: Theoretical Analysis and Efficient Implementation, IEEE Transactions on Circuits and Systems II (Early Access), doi: 10.1109/TCSII.2021.3108846.
[16] R. D. Hawkins, et al., Classical conditioning, differential conditioning, and second-order conditioning of the Aplysia gill-withdrawal reflex in a simplified mantle organ preparation, Behav. Neurosci., vol 112, no. 3, pp. 636-645, 1998.
[17] T. J. Carew, et al., Differential classical conditioning of a defensive withdrawal reflex in Aplysia californica, Science, vol. 219, no. 4583, pp. 397-400, 1983.
[18] Masato Ishikawa and Hiroyuki Torikai, Asynchronous Cellular Automaton Soma-Dendrite-Spine Model: Propagations of Action Potentials and Synaptic Plasticity, in Proc. NOLTA, paper Id 9169, 2019.